VII International Conference on Computational Methods in Marine Engineering
MARINE 2017
M. Visonneau, P. Queutey and D. Le Touzé (Eds)

GRID GENERATION FOR WALL-MODELLED LES OF SHIP HYDRODYNAMICS IN MODEL SCALE

M. LIEFVENDAHL*, M. JOHANSSON* AND M. QUAS*

*Swedish Defense Research Agency (FOI)
164 90 Stockholm, Sweden
e-mail: mattias.liefvendahl@foi.se, web page: http://www.foi.se

Key words: Wall-Modelled Large-Eddy Simulation, Ship Hydrodynamics, Grid Generation

Abstract. An unstructured grid generation approach for wall-modelled LES is proposed. The applicability of the approach is demonstrated for the simulation of the flow around an axisymmetric body, at Re-number $5.48 \cdot 10^6$, which is representable of model scale ship hydrodynamics. A numerical trip wire must be employed to induce resolved fluctuations in the simulated boundary layer. The predictive accuracy of the simulation technique is evaluated for the flow around the axisymmetric body, and for the computation of a turbulent boundary layer on a flat plate. For the flat plate, comparison is made with results from direct numerical simulation. For the axisymmetric body, results from wall-modelled LES, RANS and experimental measurements are compared.

1 INTRODUCTION

In the application of large-eddy simulation (LES) to ship hydrodynamics, the treatment of the turbulent boundary layer (TBL) along the hull is often of critical importance. The resulting computational cost is strongly dependent on the choice of the modelling technique for the TBL, and on the Reynolds (Re-)number of the simulated case. A fully developed TBL, as for instance along a ship hull, can be characterized by its thickness δ, and its viscous length scale, $\delta_\nu = (\rho\nu^2/\tau_w)^{1/2} \ll \delta$, given in terms of the density ρ, the kinematic viscosity ν, and the wall-shear stress τ_w. The most straightforward application of LES is to resolve the energetic flow structures in the inner part of the TBL, of size $\sim \delta_\nu$, which is referred to as wall-resolved LES (WRLES). If the simulation resolves the larger flow structures in the bulk of the TBL, but employs special modelling of the effects of the very near-wall flow on these larger flow structures, then the approach is referred to as wall-modelled LES (WMLES). In section 2, this classification is elaborated on, and implications for the generation of the computational grid for WMLES are discussed.

The present paper is concerned with WMLES applied to ship model scale simulations, which implies a range of hull-length based Re-numbers from 10^6 to 10^7. It is estimated [13], that WMLES would, at least, require in the order of $20 \cdot 10^6$ grid points for a simulation of the hull boundary layer. The corresponding estimate for WRLES is $\sim 10^9$ grid points. Recently

the first WRLES simulation of a ship in model scale was reported, [20]. Desipte the fact that WMLES would require significantly less computational resources, there is a striking lack in the literature of reported ship simulations of this type. There are many simulations using DES or hybrid RANS/LES methods, see e.g. [29, 9, 12, 15], but for these the entire TBL is treated in the RANS sense. For the past three decades, there has been a range of more fundamental papers on WMLES, where channel flow has been the dominating simulation case, see e.g. [22, 18] and the review of wall models in [24]. An example of an application to a geometry more complicated than an othogonal box (as for the channel flow) is the airfoil simulation reported in [2].

The main contribution of the present paper is to describe and demonstrate an unstructured grid generation approach for WMLES, which is suitable for model scale ship hydrodynamics. The guiding principle is to adapt the grid refinement level to δ, which is estimated a priori. In Section 2, estimates of the TBL length scales are first reviewed, and then the grid generation approach is described by its application to the simulation of the flow around an axisymmetric body. Results from two simulation cases are also included to in the paper to provide information concerning the predictive accuracy of WMLES. The first case, see Section 4, consists of a TBL developing over a flat plate. Results from WMLES are compared with DNS (direct numerical simulation) for validation. The second case, presented in Section 5, is the flow around the axisymmetric body, for which the grid generation approach was presented. WMLES results are compared with experimental measurements of skin friction and the mean velocity distribution in the stern region. A brief review is included in Section 3, of the turbulence modelling and numerical methods which are employed in the two simulations cases.

2 GRID REQUIREMENT ESTIMATES AND IMPLICATIONS FOR GRID GENERATION

A convenient starting point for discussing grid generation for WMLES is to estimate the number of grid points required to represent the relevant flow scales. In an early paper [3], estimates were derived for WMLES, as well as for DNS and WRLES. In subsequent papers, [27, 4, 23], the estimates, and the employed expressions for TBL thickness and friction coefficient, were refined. The relevant material is reviewed here, before the practical grid generation is described.

Consider a (material) surface S over which there is an attached TBL (no-slip boundary condition and TBL on one side of S). Locally, at a point $\mathbf{x}$ on the surface, there is TBL thickness $\delta(\mathbf{x})$ and a viscous length scale $\delta_\nu(\mathbf{x})$. Estimates for these can be obtained by correlating power law expressions to available results from DNS and experiments, see e.g. [23].

2.1 Length-scale estimates for a TBL over a flat plate

For a zero pressure gradient flat plate TBL (ZPGFPTBL), the following relations, or power laws, were used in [23].

$$\frac{\delta(x)}{x} = \alpha_1 \mathrm{Re}_x^{-\beta_1} \qquad c_f = \alpha_2 \mathrm{Re}_x^{-\beta_2} \qquad \delta_\nu = \frac{\nu}{V_0}\left(\frac{2}{c_f}\right)^{1/2} \tag{1}$$

Here δ is the wall distance at which the mean velocity is 99% of the free-stream velocity, x is the distance from the leading edge of the flat plate, V_0 is the free-stream velocity, $c_f = 2\tau_w/(\rho V_0^2)$

is the friction coefficient, and $\mathrm{Re}_x = xV_0/\nu$. The model coefficent values,

$$\alpha_1 = 0.1222, \qquad \beta_1 = 0.1372, \qquad \alpha_2 = 0.0283, \qquad \beta_2 = 0.1540, \tag{2}$$

were obtained by correlation with experimental data [21]. A comparison with a compilation of experimental data [17], and DNS [25, 26] showed that the expressions (1) are quite accurate in the range, $10^6 < \mathrm{Re}_x < 5 \cdot 10^7$.

As an example, we apply the expressions for δ and δ_ν to the TBL mid-ships in a typical model scale experiment. Assuming a model length of $L = 5\,\mathrm{m}$, a towing speed $V_0 = 2\,\mathrm{m/s}$, and a kinematic viscosity $\nu = 10^{-6}\,\mathrm{m}^2/\mathrm{s}$, gives $\mathrm{Re}_x = 5 \cdot 10^6$. For these parameters, the expressions (1) give $\delta = 37\,\mathrm{mm}$, and $\delta_\nu = 14\,\mu\mathrm{m}$, i.e. $\delta/\delta_\nu \approx 2\,700$. It is quite clear that a great gain in computational cost can be achieved if the grid is constructed to resolve δ and not δ_ν, i.e. by using WMLES instead of WRLES.

2.2 Grid estimates for WMLES

The fundamental assumption in the present paper is that the grid for WMLES should be adapted to δ. This is translated to a requirement of a fixed number of grid points n_0 in a δ^3-cube of the TBL. Values in the range, $500 < n_0 < 10^4$ have been reported in the literature [3, 27, 5]. See also sections 4 and 5 below for practical demonstrations grid resolution and achieved predicitive accuracy. This means that we have a local density of grid points, $\rho_N(\mathbf{x}) = n_0/\delta(\mathbf{x})^3$, and we obtain the total number of grid points N by integrating this over the TBL at the surface S.

$$N = \int_S \int_0^{\delta(\mathbf{x})} \rho_N(\mathbf{x})\,\mathrm{d}y\mathrm{d}S = \int_S \frac{n_0}{\delta(\mathbf{x})^2}\,\mathrm{d}S \tag{3}$$

Here y is the local wall-normal coordinate, with $y = 0$ at the wall. A number of observations concerning expression (3) can be made:

1. The grid estimates, [3, 27, 4, 23], were obtained by inserting a power law for δ which is valid for a FPZPGTBL. It is referred to the original papers for the derivation, and the resulting grid estimates.

2. The integral (3) is only valid for a fully developed TBL. Its initial section, comprising the laminar boundary layer and its transition to turbulence, must be handled separately.

3. The integral (3) only covers the TBL-region. Grid estimates for the region of the flow away from the wall/TBL must be handled separately.

The practical implications of these observations are discussed in the next section, and in connection with the two simulation cases included in the paper.

2.3 Grid generation

A grid generation method for WMLES is demonstrated by applying it for the construction of a computational grid for the computation of the external flow around the axisymmetric body shown in Fig. 1. The body is the unappended bare hull geometry of the generic submarine design proposed in [10, 11], see also [1]. The grid is to be constructed for flow at a length-based

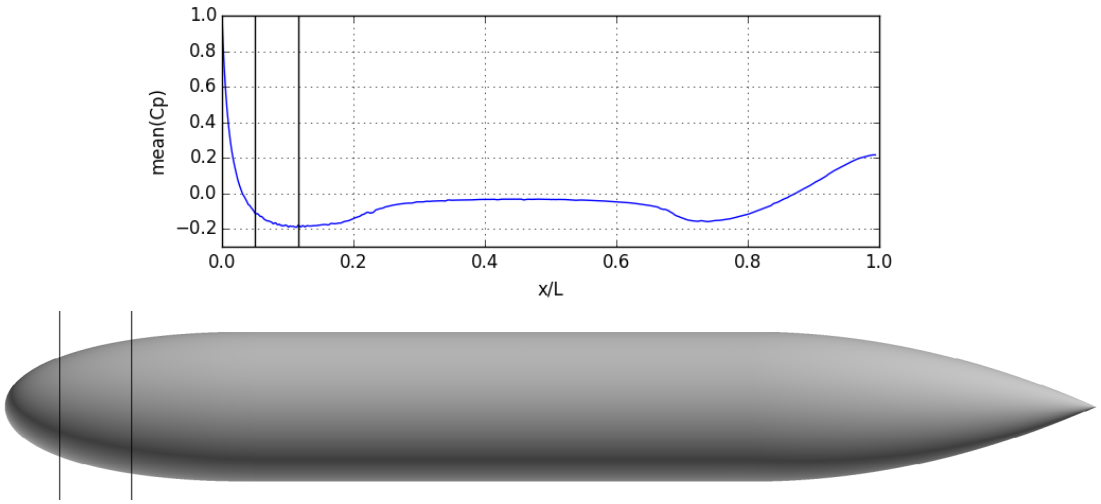

Figure 1: The axisymmetric body. Bow to the left and stern to the right. Above: Mean pressure coefficient as a function of x/L. The left-most vertical black line, $x/L = 0.050$, indicates the location of the trip-wire. The second vertical black line, $x/L = 0.116$, indicates the pressure minimum on the bow.

Re-number, $LV_0/\nu = 5.48 \cdot 10^6$, see Table 2 for the complete set of parameters of the simulated case, and Section 5 for a description of the simulation results.

The boundary layer over the hull starts at the stagnation point on the bow and develops first as laminar, affected by a favorable pressure gradient. The pressure coefficient on the hull is also shown in Fig. 1. Generally, a favorable pressure gradient has a stabilizing effect, whereas an adverse pressure gradient supports transition. The simulated case corresponds to wind tunnel measurements, see section 5, in which a trip wire was included to fix the location of the boundary layer transition. The location of the trip wire, $x/L = 0.05$, is shown in Fig. 1. Here the x-coordinate is directed in the main flow direction, and $x = 0$ at the stagnation point. Downstream of the trip wire, the boundary layer is turbulent and it is attached to and develops along the hull. At the stern, the TBL is affected by an adverse pressure gradient which leads to a rapid thickening of the TBL. There is no separation of the mean flow at the stern. As can be seen in Fig. 1, the pressure gradient is relatively weak downstream of the location of the trip wire. In the WMLES computation, a numerical trip wire is employed at the same location as the trip wire used in the experiments.

The objective is now to construct an unstructured grid which is adapted to the local thickness of the TBL. From now on the discussion is in terms of a grid for finite volume discretization of the governing equations over the grid cells. The general approach however is applicable also in other numerical frameworks such as the finite element method. In the chosen approach the following three steps are carried out in order to create the complete grid of the computational domain.

1. The hull surface is grid is first created by triangulating the surface.

2. A certain number of layers of prismatic cells are extruded from the surface triangulation.

3. A tetrahedral grid is generated for the domain outside of the layers of prismatic cells.

The adaption of the cell size to the local TBL thickness is primarily done at the first stage, the surface meshing. The assumed variation of the TBL thickness is given by the following expression.

$$\delta(x) = \begin{cases} \delta_0 & , x < x_1 \\ \alpha_1 x \mathrm{Re}_x^{-\beta_1} & , x \geq x_1 \end{cases} \tag{4}$$

Here x_1 is chosen at a suitable location just downstream of the trip wire, at $x/L \approx 0.06$, and δ_0 is chosen to have continuity of the function $\delta(x)$ at x_1. This is next translated to a recommended cell/triangle edge length Δl by the relation,

$$\left(\frac{\delta}{\Delta l}\right)^3 = n_0, \tag{5}$$

which corresponds to n_0 cubical cells in the (local) δ^3-cube. It would be possible to include a constant factor in equation (5) to account for the difference in using tet/prism cells, and not cubical cells. This would however exactly correspond simply to a scaling of n_0.

Now parameters are chosen for the grid generation for the simulation for which results are presented in Section 5. The values $\delta_0 = 4\,\mathrm{mm}$, and $n_0 = 500$, are chosen. This leads to a recommended edge length of, $\Delta l \approx 0.5\,\mathrm{mm}$, for the triangles of the grid over the bow. The gradual increas of $\delta(x)$ downstream of x_1 leads to a thickness of $\delta \approx 15\,\mathrm{mm}$, at the end of the parallel section of the hull, which corresponds to $\Delta l \approx 2\,\mathrm{mm}$, at this station. The total number of triangles in the resulting surface mesh is approximately $1.25 \cdot 10^6$.

The second step is to extrude prismatic cells from the surface triangulation. The cells are constructed with a height aspect ratio of, $\Delta h/\Delta l \approx 0.5$, and 16 layers are created without any expansion ratio away from the wall. This leads to a prismatic TBL grid covering approximately the full width δ. The total cell count of the TBL grid is $20.5 \cdot 10^6$ prisms.

The third and last step is to construct a tetrahedral grid for the remainder of the computational domain. In the present case, the focus of the investigation is the TBL. Hence, no special regions with increased grid density are needed, and it is possible to rapidly coarsen the mesh away from the TBL. The generated grid contains $5.7 \cdot 10^6$ tetrahedral cells, leading to a total grid cell count of $26.3 \cdot 10^6$.

3 CFD METHODS

The turbulence modelling and numerical methods employed in the two simulations, presented in Sections 4 and 5 respectively, are briefly summarized in this section, and references are given to complete descriptions.

3.1 Large-eddy simulation

Spatial filtering of the incompressible Navier-Stokes equations, and neglecting commutation errors, lead to the fundamental LES equations, see e.g. [24]:

$$\begin{aligned} \frac{\partial \overline{\mathbf{v}}}{\partial t} + \nabla \cdot (\overline{\mathbf{v}} \otimes \overline{\mathbf{v}}) &= -\frac{1}{\rho}\nabla \overline{p} + \nabla \cdot (\overline{\mathbf{S}} - \mathbf{B}) \\ \nabla \cdot \overline{\mathbf{v}} &= 0 \end{aligned} \tag{6}$$

Here $\overline{\mathbf{v}}$ is the (filtered) velocity field, ρ the density, $\overline{p}$ the pressure, $\overline{\mathbf{S}} = 2\nu\overline{\mathbf{D}}$ the viscous strain tensor, $\overline{\mathbf{D}} = (\nabla\overline{\mathbf{v}} + \nabla\overline{\mathbf{v}}^T)/2$ the rate-of-strain tensor and ν the kinematic viscosity. The term in equation (7) arising from the filtering, is the subgrid stress tensor, $\mathbf{B} = \overline{\mathbf{v} \otimes \mathbf{v}} - \overline{\mathbf{v}} \otimes \overline{\mathbf{v}}$. Here, variables with overbar denotes filtered quantities. Below however, the overbar is dropped in order to simplify the notation. It is referred to [24] as a general reference for LES and [8], and the references therein, for LES applied to problems in naval hydrodynamics.

The LES modelling consists of providing an expression for $\mathbf{B}$. In the simulations reported below, the wall-adapting local eddy viscosity (WALE) model, by Nicoud and Ducros [19], is employed. This is an eddy-viscosity model, which means that the subgrid stress is computed as $\mathbf{B} = -2\nu_k\overline{\mathbf{D}}$, where ν_k is the subgrid viscosity. In the WALE model, ν_k is determined using an expression including the velocity gradient tensor.

For the flow next to the wall, special subgrid modelling must be used in the form of a so-called wall model. The one employed in the simulations of this paper uses the cell-centered velocity in cells adjacent to the wall, and the expression for the law-of-the wall by Spalding [28], to enforce the correct wall-shear stress in each time step. It is referred to [6, 7, 14] for complete description of this wall model.

3.2 The finite volume discretization

The solver which is used is implemented using the open source software package OpenFOAM[1], which provides an object-oriented library, based on the finite-volume method, specifically designed for CFD, see [30] for the original description of the structure of this software design. The LES subgrid models have been implemented inhouse at FOI.

The discretization of the governing flow equations relies on storage of the unknown flow variables in the cell-center positions in the computational grid. The algorithm supports arbitrary polyhedral cells and the grid is treated as unstructured. The approximations involved are of second-order accuracy, except for flux limiting for the convective term, which reduces locally the formal order of accuracy near sharp gradients. The momentum equation is treated in a segregated manner, solving sequentially the three components of the momentum equations in a loop within each time step.

The simulations are time resolved and a second order backward differencing scheme is used for the time advancement of the components of the momentum equation. A domain decomposition technique, applied to the grid, in combination with an efficient MPI-implementation is used for running on parallel computers.

4 FLAT PLATE TURBULENT BOUNDARY LAYER

The turbulent boundary layer over a flat plate is simulated using WMLES at a length-based $\mathrm{Re} = 2.47 \cdot 10^6$. The predictive accuracy is evaluated by comparison with DNS-results. For the WMLES, a block-structured grid with uniform hexahedral cells is used in the rectangular simulation domain. Hence the unstructured grid generation approach described above is not used for this case. Nevertheless, the simulated case provides useful information concerning the predictive accuracy of WMLES, with a reasonable grid resolution relative to the TBL thickness. The case is especially useful because of the availability of DNS-data for validation.

[1] `www.openfoam.com`

Table 1: Physical parameters for the flat plate simulation case.

Quantity	Notation	Value	Unit
Plate length	L	2.002	m
Channel height	h	0.133	m
Plate width	b	0.200	m
Kinematic viscosity	ν	$1.65{\cdot}10^{-5}$	m^2/s
Free-stream velocity	V_0	20.4	m/s
Reynolds number	$\mathrm{Re} = V_0 L/\nu$	$2.47{\cdot}10^{6}$	- - -

4.1 Parameters, pre-processing and simulation

The physical parameters of the flat-plate case are summarized in Table 1. The flow takes place in a rectangular domain,

$$(x, y, z) \in [0, L] \times [0, h] \times [0, b],$$

where L is the length of the plate, b is the width of the plate, h is the height of the simulation domain (channel), and the main flow is in the x-direction. A uniform inflow velocity, V_0, is prescribed at the inflow at $x = 0$. The plate is the bottom of the channel, $y = 0$, at which no-slip boundary conditions are applied. At the top boundary, $y = h$, a slip boundary condition is applied, and in the z-direction periodic boundary conditions are employed. A simple orthogonal grid was used, with $760 \times 160 \times 100 = 12\,160\,000$ uniform hexahedral cells.

One WMLES computation was carried out using the WALE subgrid model. It is referred to Section 3 for a description of the wall model and the numerical methods. In order to induce resolved fluctuations in the boundary layer, a numerical trip wire is applied on the plate, next to the inflow. This is affecting the flow through a random volume force applied in a strip of cells next to the plate.

4.2 Results for the flat plate

The flow over the flat plate, simulated by WMLES, is illustrated in Fig. 2, which shows the instantaneous axial velocity and the wall shear stress on the plate. At two locations, one near the inflow and one near the outflow, the grid resolution relative to the length scales of the flow structures is also illustrated. For this simulation, naturally, the grid resolution relative to the TBL is increasing because of the uniform cell size and the growing thickness of the TBL along the plate.

The development of the mean friction coefficient and the momentum thickness, θ, of the TBL are shown in Fig. 3. The WMLES-results are compared with the power law expression for c_f, see equation (1). In the absence of a pressure gradient, the relation, $c_f = 2\mathrm{d}\theta/\mathrm{d}x$, holds and can be integrated to yield a power law for θ. Good agreement is seen between the WMLES and the power law. The "wiggles" in c_f at, $x \approx 0.15$, is related to the numerical trip wire and the development of resolved fluctuations in the simulation. The θ-curve for WMLES is shifted in the x-direction relative to the power law. This is also explained by the initial development of the TBL. After this initial section, the WMLES-results demonstrate the corrected TBL-thickness growth.

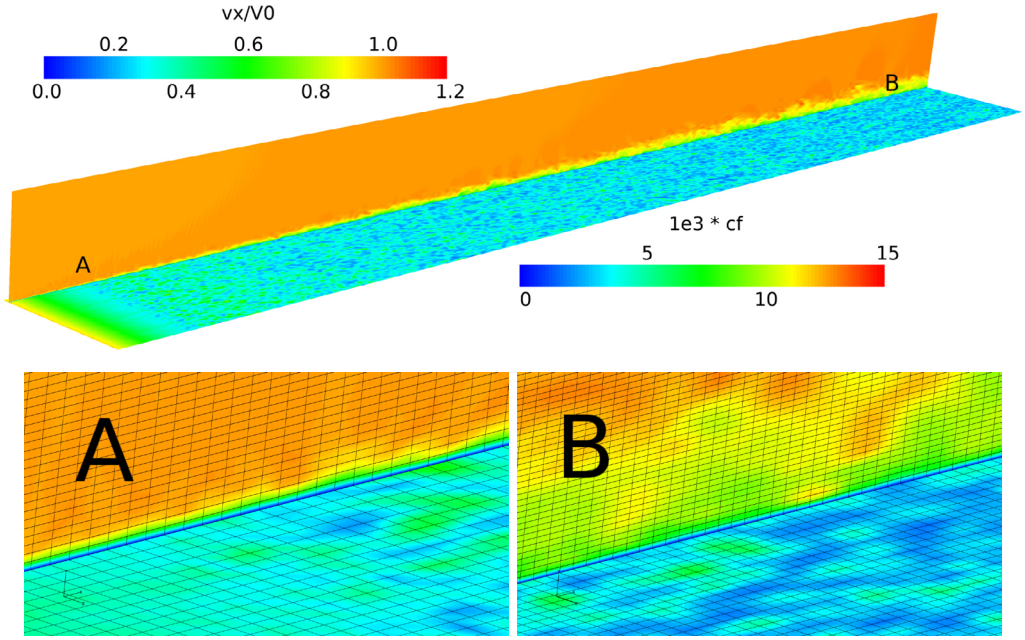

Figure 2: The flat-plate TBL simulated by WMLES. On the bottom wall, the friction coefficient, $10^3 \cdot c_f$, is plotted, and on a vertical plane the normalized instantaneous velocity, v_x/V_0, is plotted. The above graph shows the whole channel. The two pictures below are zoomed-in at the locations marked by 'A' and 'B' respectively. In the below pictures, the grid is also shown on the bottom wall and the vertical plane.

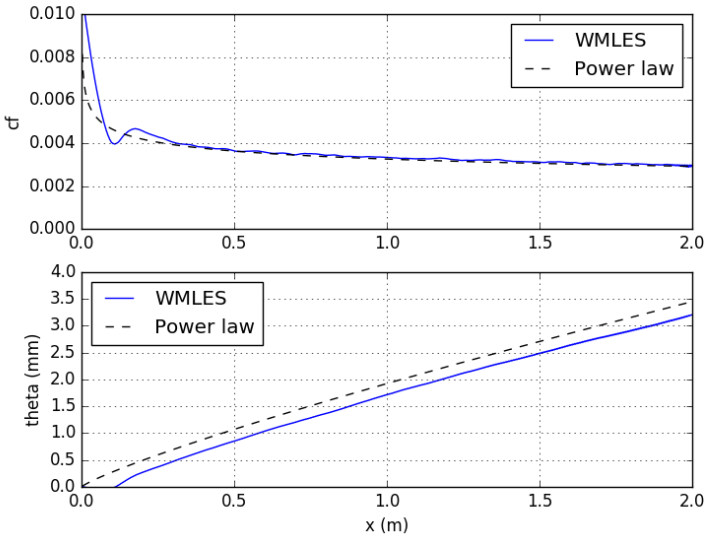

Figure 3: Mean friction coefficient and momentum thickness of the flat plate TBL. Comparison of WMLES-results with the power laws (1). Above: Mean friction coefficient, $\langle c_f \rangle$, as a function of x. Below: TBL momentum thickness, θ, as a function of x.

Profiles of flow statistics are shown in Fig. 4. WMLES-results are compared with DNS, see [25], at a station corresponding to, $\theta V_0/\nu = 3\,626$. For the WMLES-computation, this station is located at, $x = 1.76\,\text{m}$, i.e. relatively near the outlet. The grid cell height is, $\Delta y = 0.8\,\text{mm}$, which at this station corresponds to, $\Delta y^+ = \Delta y/\delta_\nu \approx 41$, based on the viscous length scale calculated by WMLES. The first cell center is thus located at, $y^+ \approx 20$, and the mean velocity is, $\langle v_x \rangle \approx 0.45 V_0$, in this point. Considering the level of grid resolution, the agreement of the profiles can be considered to be relatively good. The peak value of the turbulent shear stress is well predicted. The main discrepancy is that the turbulent stress profile decays too slowly at away from the wall. This is associated with large TBL flow structures which intermittently reaches out to a wall distance of 25-30 mm in the WMLES. Based on a boundary layer thickness of $\delta \approx 3\,\text{mm}$, the grid resolution at this station is $\approx$5 000 cells in a δ^3-cube. This can be considered as relatively high. The TBL prediction is however affected by the development of the TBL along the plate where the grid resolution relative to δ is lower.

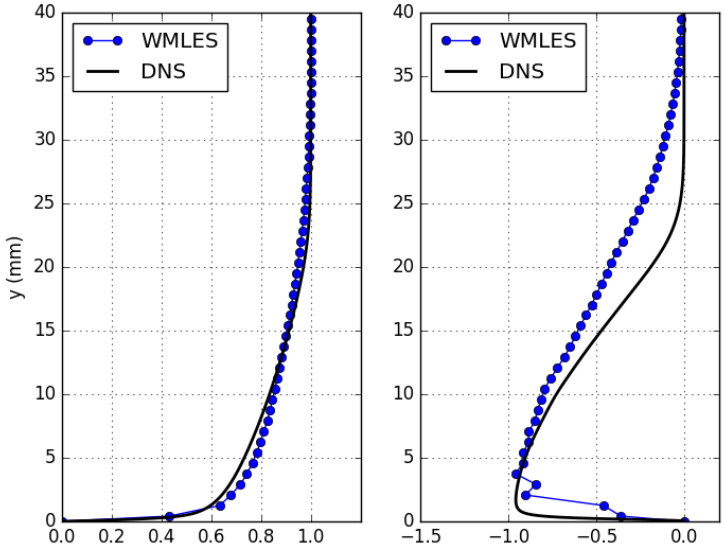

Figure 4: Profiles of mean axial velocity, $\langle v_x \rangle / V_0$ (left), and the turbulent shear stress, $\langle v_x' v_y' / u_\tau^2 \rangle$ (right), at $\text{Re}_\theta = 3\,626$. On the vertical axis, the wall-distance y is found. Comparison of WMLES-results with DNS, [25].

5 FLOW AROUND AN AXISYMMETRIC BODY

The flow around an axisymmetric model in a wind-tunnel is simulated using WMLES at a length-based $\text{Re} = 5.48 \cdot 10^6$. The results are compared with measurements of the skin friction and the mean velocity at the stern and in the near wake. The grid generation approach described in the Section 2.3 was employed for the simulation.

5.1 Parameters, pre-processing and simulations

The physical parameters of the axisymmetric body simulation case are summarized in Table 2. This corresponds to experiments carried out in the DSTO low speed wind tunnel, [1]. A

Cartesian coordinate system is used with the main flow in the positive x-direction and, $x = 0$, at the bow of the body. The flow is simulated in a rectangular computational domain, occupying, $-1.25\,\mathrm{m} < x < 6.44\,\mathrm{m}$, and with cross-section, $1.92\mathrm{m} \times 1.92\mathrm{m}$. At the inlet, the constant flow velocity $V_0 = 60\,\mathrm{m/s}$, is prescribed.

Table 2: Physical parameters for the axisymmetric body simulation case.

Quantity	Notation	Value	Unit
Hull length	L	1.350	m
Hull diameter	D	0.185	m
Kinematic viscosity	ν	$1.478 \cdot 10^{-5}$	m^2/s
Free-stream velocity	V_0	60.0	m/s
Reynolds number	$\mathrm{Re} = V_0 L/\nu$	$5.48 \cdot 10^6$	- - -

One WMLES computation was carried out using the WALE subgrid model on a grid generated according to the procedure described in Section 2.3, with a total of $26 \cdot 10^6$ cells. To induced resolved fluctuations, a numerical trip wire was employed on the bow of the body, as described in Section 2.3. For comparison, the flow was also simulated using the $k - \omega$ SST turbulence model, [16], as implemented in the standard OpenFOAM-solver `simpleFoam`.

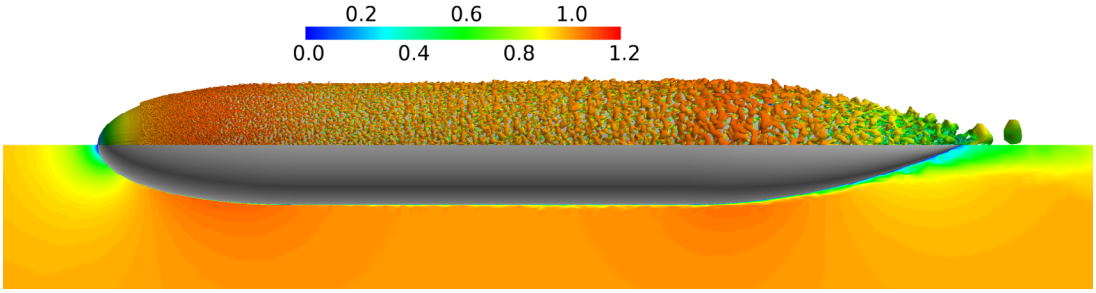

Figure 5: Visualization of the flow around the axisymmetric body simulated using WMLES. In the top half, an iso-surface of the second invariant of the velocity gradient is shown, illustrating the resolved fluctuations in the TBL. In the lower half, the normalized axial velocity, v_x/V_0, is shown on the center plane. The iso-surface is also colored by v_x/V_0, using the same color scale.

5.2 Results for the axisymmetric body

The flow around the axisymmetric body, simulated by WMLES, is illustrated in Fig. 5. There are resolved fluctuations in the TBL over the complete hull downstream of the trip wire. The skin friction along the body is plotted in Fig. 6. The measurement were obtained using the Preston tube method, see [1] and the references therein for more information. The qualitative behaviour of the three c_f-curves is quite similar. The results indicate an underprediction with $\approx 30\%$ for WMLES as compared to the measurements. This may be associated with a thinner TBL in the WMLES simulation. The cause for this may be related to the action of the trip wire or the mesh resolution relative to the TBL. This discrepancy does not however appear to have

a significant effect on the thickening of the TBL over the stern, and the formation of the wake, as discussed next.

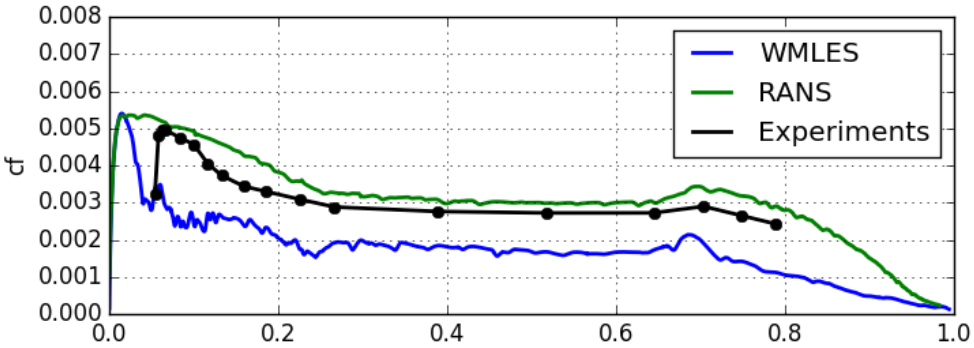

Figure 6: Mean friction coefficient, $\langle c_f \rangle$, as a function of x/L along the axisymmetric body. Comparison of results from WMLES, RANS and measurements, [1].

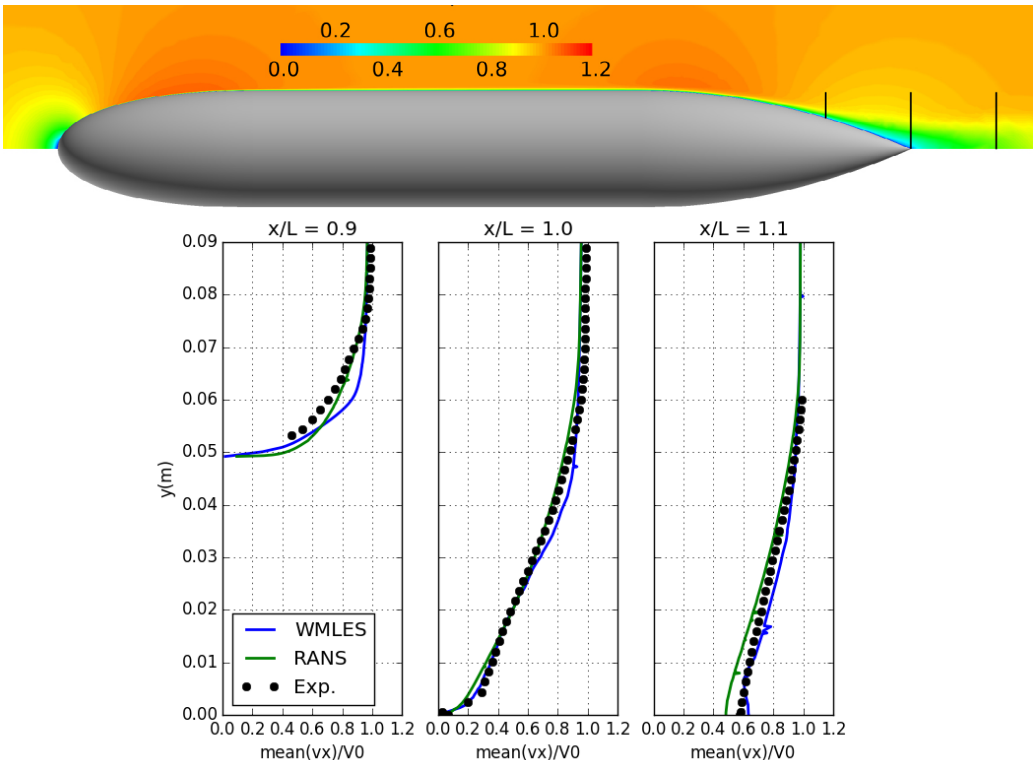

Figure 7: Comparison of profiles of the mean axial velocity, $\langle v_x \rangle / V_0$, obtained by WMLES, RANS and measurements, [1], respectively. The top graph illustrates the three lines (black) along which the profiles have been extracted, at $x/L = 0.9$, 1.0 and 1.1 respectively. The vertical axis in the three profile plots is the vertical coordinate y (with $y = 0$ on the symmetry axis of the body).

The mean velocity at the stern and in the near wake is shown in Fig, 7. Mean velocity profiles are extracted at three stations, and results are compared from WMLES, RANS and measurements. Hot wire anemometry was used in the measurements, see [1] and the references therein for more information. At the first station, $x/L = 0.9$, when the adverse pressure gradient has just started to affect the TBL, there are noticeable differences between the profiles. The measurements cannot reach very close to the surface, and there also appear to be a slight displacement of the measured profile out from the boundary. The WMLES profile, at $x/L = 0.9$, is most likely too thin, which would correlate well with the observation concerning the underprediction of c_f above. Nevertheless, there is a quite good agreement between all three sets of results for the profiles at the stern, $x/L = 1.0$, and in the near wake, $x/L = 1.1$. This is an indication that WMLES may be robust for prediction of the flow away from walls, even if the TBL is not well resolved, $n_0 = 500$ for the present case, or very accurately represented.

6 CONCLUSIONS

An unstructured grid generation approach for WMLES, suitable for model scale ship hydrodynamics, have been described, see Section 2.3, and demonstrated for the simulation of the flow around an axisymmetric model, see Section 5. The main feature of the proposed approach is to adapt the grid to the local TBL thickness, which is estimated a priori. An essential component of the method is to employ a numerical trip wire in order to induce resolved fluctuations in the boundary layer. Aspects of the placement of the numerical trip and the requirements on the grid in this region are also discussed. There is potentially a great gain in computational cost if WMLES can be applied instead of WRLES. In the WMLES of the axisymmteric body, $26 \cdot 10^6$ grid cells were used, whereas the it is estimated that WRLES for the same case would require in the order of 10^9 cells, [23].

The predictive accuracy of the overall WMLES approach is evaluated by its application to two simulation cases: (i) The turbulent boundary layer over a flat plat, and (ii) The flow around an axisymmtric body. For the flat plate, the results are validated by comparison with DNS. For the axisymmetric body, results are compared between WMLES, RANS and experimental measurements. Integral quantities, such as skin friction and TBL thickness, are included in the evaluation, as well as profiles of the mean velocity and the turbulent shear stress. The overall conclusion is that WMLES, with the proposed unstructured grid generation approch, is promising for model scale ship hydrodynamics. The predictive accuracy is relatively good, and the computational cost is well within the scope of many current medium scale high-performance computing systems.

REFERENCES

[1] B. Anderson, M. Chapuis, L. Erm, C. Fureby, M. Giacobello, S. Henbest, D. Jones, M. Jones, C. Kumar, M. Liefvendahl, P. Manovski, D. Norrison, H. Quick, A. Snowden, A. Valiyff, R. Widjaja, and B. Woodyatt. Experimental and computational investigation of a generic conventional submarine hull form. In *29th Symposium on Naval Hydrodynamics*, Gteborg, Sweden, August 2012.

[2] S. T. Bose and P. Moin. A dynamic slip boundary condition for wall-modeled large-eddy simulation. *Physics of Fluids*, 26(015104):1–18, 2014.

[3] D. R. Chapman. Computational aerodynamics development and outlook. *AIAA Journal*, 17:1293–1313, 1979.

[4] H. Choi and P. Moin. Grid-point requirements for large-eddy simulation: Chapman's estimates revisited. Technical Report Annual research briefs, Center for Turbulence Research, Stanford University, 2011.

[5] L. Davidson. Large Eddy Simulation: How to evaluate resolution. *International Journal of Heat and Fluid Flow*, 30:1016–1025, 2009.

[6] E. de Villiers. *The potential of large-eddy simulation for the modeling of wall-bounded flows.* PhD thesis, Imperial College London, 2006.

[7] C. Fureby. On LES and DES of Wall Bounded Flows. ERCOFTAC Bulletin, March 2007.

[8] C. Fureby. Large Eddy Simulation of Ship Hydrodynamics. In *27th Symposium on Naval Hydrodynamics*, Seoul, Korea, October 2008.

[9] C. Fureby, S. L. Toxopeus, M. Johansson, M. Tormalm, and K. Petterson. A computational study of the flow around the KVLCC2 model hull at straight ahead conditions and at drift. *Ocean Engineering*, 118:1–16, 2016.

[10] P. N. Joubert. Some Aspects of Submarine Design. Part 1, Hydrodynamics. Technical Report DSTO-TR-1622, Defence Science and Technology Organisation, Australia, 2004.

[11] P. N. Joubert. Some Aspects of Submarine Design. Part 2, Shape of a Submarine 2026. Technical Report DSTO-TR-1920, Defence Science and Technology Organisation, Australia, 2006.

[12] M. Liefvendahl, N. Alin, M. Chapuis, C. Fureby, U. Svennberg, and C. Troëng. Ship and propulsor hydrodynamics. In *V European Conference on Computational Fluid Dynamics, ECCOMAS CFD2010*, Lissabon, Portugal, 2010.

[13] M. Liefvendahl, C. Fureby, and O. J. Boelens. Grid Requirements for LES of Ship Hydrodynamics in Model and Full Scale. In *31st Sympositum on Naval Hydrodynamics*, Moneterey, California, September 2016.

[14] M. Liefvendahl, T. Mukha, and S. Rezaeiravesh. Formulation of a Wall Model for LES in a Collocated Finite-Volume Framework. Technical Report 2017-001, Department of Informtion Technology, Uppsala University, 2017.

[15] J. E. Martin, M. Esmaeilpour, and P. M. Carrica. Near-Field Wake of Surface Ships and Submarines Operating in a Stratified Fluid. In *31st Symposium on Naval Hydrodynamics*, Monterey, USA, September 2016.

[16] F. R. Menter. Two-equation eddy-viscosity turbulence models for engineering applications. *AIAA Journal*, 32(8):1598–1605, 1994.

[17] H. M. Nagib, K. A. Chauhan, and P. A. Monkewitz. Approach to an asymptotic state for zero pressure gradient turbulent boundary layers. *Phil. Trans. R. Soc. A*, 365:755–770, 2007.

[18] F. Nicoud, J. S. Baggett, P. Moin, and W. Cabot. Large eddy simulation wall-modeling based on suboptimal control theory and linear stochastic estimation. *Physics of Fluids*, 13(10), 2001.

[19] F. Nicoud and F. Ducros. Subgrid-scale stress modeling based on the square of the velocity gradient. *Flow, Turbulence and Combustion*, 63:183–200, 1999.

[20] T. Nishikawa, Y. Yamade, M. Sakuma, and C. Kato. Application of Fully-resolved Large Eddy Simulation to KVLCC2. *Journal of the Japan Society of Naval Architects and Ocean Engineers*, 16:1–9, 2012.

[21] J M Österlund. *Experimental studies of zero pressure-gradient turbulent boundary layer flow*. PhD thesis, Department of Mechanics, Royal Institute of Technology, Stockholm, 1999.

[22] U. Piomelli, J. Ferziger, P. Moin, and J. Kim. New approximate boundary conditions for large-eddy simulations of wall-bounded flows. *Physics of Fluids A*, 1(6):1061–1068, 1989.

[23] S. Rezaeiravesh, M. Liefvendahl, and C. Fureby. On grid resolution requirements for LES of wall-bounded flows. In *VII European Congress on Computational Methods in Applied Sciences and Engineering*, Crete, Greece, June 2016.

[24] P. Sagaut. *Large eddy simulation for incompressible flows*. Springer-Verlag, 2 edition, 2002.

[25] P. Schlatter and R. Örlü. Assessment of direct numerical simulation data of turbulent boundary layers. *J. Fluid Mech.*, 659:116–126, 2010.

[26] J A Sillero, Jiménez, and R D Moser. One-point statistics for turbulent wall-bounded flows at Reynolds numbers up to $\delta^+ \approx 2000$. *Phys. Fluids*, 25(105102), 2013.

[27] P. R. Spalart, W.-H. Jou, M. Strelets, and S. R. Allmaras. Comments on the feasibility of LES for wings and on a hybrid RANS/LES approach. In C. Liu and Z. Liu, editors, *Advances in DNS/LES. Proceedings of the First AFOSR International Conference on DNS/LES*. Greyden Press, 1997.

[28] D. B. Spalding. A Single Formula for the "Law of the Wall". *Journal of Applied Mechanics*, pages 455–458, 1961.

[29] M. Visonneau, G. Deng, E. Guilmineau, P. Queutey, and J. Wackers. Local and global assessment of the flow around the japan bulk carrier with and without energy saving devices at model and full scale. In *31st Symposium on Naval Hydrodynamics*, Monterey CA, USA, 2016.

[30] H. G. Weller, G. Tabor, H. Jasak, and C. Fureby. A tensorial approach to computational continuum mechanics using object-oriented techniques. *Computers in Physics*, 12(9):620–631, 1998.